GLOBAL JOURNAL
OF RESEARCH IN ENGINEERING - F: ELECTRICAL & ELECTRONIC

Volume 26 | 2026 Article ID: GJRE-274142 Language: English

Joint Sequential use of the Reassigned Smoothed Pseudo Wigner-Ville Distribution and the Hough Transform vs. the Reassigned Smoothed Pseudo Wigner-Ville Distribution for Detecting Low Probability of Intercept Frequency Shift Keying Radar Signals in High Noise Environments

Online First

Dr. Daniel L. Stevens [§] [*]

[*]Corresponding Author

Solomon O. Stevens [‡]

[§] Air Force Research Laboratory, Rome, United States
[‡] Northwest Missouri State University [(OA)]

RECEIVED	ACCEPTED	ONLINE PUBLISHED	PEER REVIEW
2026-08-09	2026-08-18	2026-09-01	Double Blind

Abstract

Digital intercept receivers have moved away from Fourier-based analysis techniques, towards classical time-frequency analysis techniques, for the purpose of analyzing low probability of intercept radar signals. This paper presents the novel approach of detecting low probability of intercept frequency shift keying radar signals through utilization and direct comparison of the joint sequential use of the Reassigned Smoothed Pseudo Wigner Ville Distribution and the Hough Transform versus the Reassigned Smoothed Pseudo Wigner Ville Distribution. Frequency shift keying signals were analyzed. The following metrics were used for evaluation: percent detection, and lowest signal-to-noise ratio for signal detection. Experimental results demonstrate that overall, the joint sequential use of the Reassigned Smoothed Pseudo Wigner Ville Distribution and the Hough Transform produced more accurate detection metrics than the Reassigned Smoothed Pseudo Wigner Ville Distribution.

frequency shift keying | Hough transform | low SNR | LPI Radar | reassigned smoothed pseudo Wigner-Ville distribution | signal detection | Time-Frequency Analysis

AI USE STATEMENT
No generative AI was used for analysis or results.

FUNDING
No external funding was declared for this work.

CONFLICT OF INTEREST
The authors declare no conflict of interest.

DATA AVAILABILITY
Not applicable for this article.

ETHICS
No ethics committee approval was required for this article type.

CONSENT
Not applicable for this article.

TRIAL REG.
Not applicable.

Crossref DOI: 10.34257/GJREF274142

How to Cite: Stevens et al. (2026). Joint Sequential use of the Reassigned Smoothed Pseudo Wigner-Ville Distribution and the Hough Transform vs. the Reassigned Smoothed Pseudo Wigner-Ville Distribution for Detecting Low Probability of Intercept Frequency Shift Keying Radar Signals in High Noise Environments. Global Journal of Research in Engineering. Ahead of Print. DOI: 10.34257/GJREF274142

AR Experience Web Page DOI

Print ISSN 0975-5861
9 770975 586007

Online ISSN 2249-4596
9 772249 459017

Under the strict compliance and defined process of

METADATA CONTINUATION

AUTHOR CONTACT QR LEDGER

Dr. Daniel L. Stevens

Solomon O. Stevens

ARCHIVAL RECORD

GJRE · Vol 26 · Issue 1 · 2026

Article ID GJRE-274142 · DOI 10.34257/GJREF274142

Print ISSN 0975-5861 · Online ISSN 2249-4596

Global Journal of Research in Engineering - Section F
GJRE

Joint Sequential use of the Reassigned Smoothed Pseudo Wigner-Ville Distribution and the Hough Transform vs. the Reassigned Smoothed Pseudo Wigner-Ville Distribution for Detecting Low Probability of Intercept Frequency Shift Keying Radar Signals in High Noise Environments

Dr. Daniel L. Stevens§ * and Solomon O. Stevens‡

Affiliations
§ Air Force Research Laboratory, Rome, United States
‡ Northwest Missouri State University (OA)

Abstract

Digital intercept receivers have moved away from Fourier-based analysis techniques, towards classical time-frequency analysis techniques, for the purpose of analyzing low probability of intercept radar signals. This paper presents the novel approach of detecting low probability of intercept frequency shift keying radar signals through utilization and direct comparison of the joint sequential use of the Reassigned Smoothed Pseudo Wigner Ville Distribution and the Hough Transform versus the Reassigned Smoothed Pseudo Wigner Ville Distribution. Frequency shift keying signals were analyzed. The following metrics were used for evaluation: percent detection, and lowest signal-to-noise ratio for signal detection. Experimental results demonstrate that overall, the joint sequential use of the Reassigned Smoothed Pseudo Wigner Ville Distribution and the Hough Transform produced more accurate detection metrics than the Reassigned Smoothed Pseudo Wigner Ville Distribution.

Keywords: *frequency shift keying, Hough transform, low SNR, LPI Radar, reassigned smoothed pseudo Wigner-Ville distribution, signal detection, Time-Frequency Analysis*

*** Corresponding Author**
Dr. Daniel L. Stevens

DOI
10.34257/GJREF274142

1. Introduction

1.1. LPI Radar Overview

Presently, many radar users are specifying Low Probability of Intercept (LPI) as an important tactical requirement [YUA24]. The term LPI is the property of a radar that, because of its power management, ultra-low side lobes, pulse compression, and other design attributes, makes it difficult to be detected by means of intercept receivers, such as electronic support receivers, electronic intelligence receivers, and radar warning receivers [WSQ19].

Power management is the radar's ability to control the power level so that it emits only the necessary power for detection of a target. An intercept receiver is used to seeing an increase in power as the radar approaches. If a power managed LPI radar decreases the power as it approaches the target, an intercept receiver may incorrectly assume that the radar is not approaching, thereby deciding that no response management is necessary, which could be a deadly decision [SHC19].

Ultra-low side lobes are used to prevent an intercept receiver from detecting radar emissions from the side lobes of the radar. Ultra-low side lobes are generally required to be -45dB or lower [SON22].

Pulse compression is a very important LPI radar characteristic. For frequency modulation LPI radars, the transmitted Continuous Wave (CW) signal is coded with a reference signal that spreads the transmitted energy in frequency, making it more difficult for an intercept receiver to detect and identify the LPI radar. The reference signal can be a linear frequency modulated signal or a Frequency Shift Keying (FSK) (frequency hopping). The most popular implementation has been the Frequency Modulated Continuous Wave (FMCW) [LIX23].

The goal of the LPI radar is to detect targets at longer ranges than the intercept receiver can detect the LPI radar. It is important to note that defining a radar to be LPI necessitates defining the corresponding intercept receiver. That is, the success of an LPI radar is measured by how hard it is for the intercept receiver to detect and intercept the radar's emissions.

The LPI emitter has established itself as one of the premier tactical and strategic radars in the military spectrum. In addition to surveillance and navigation, the LPI emitter also operates in the time-critical domain for applications such as fire control and missile guidance [WIL06].

1.2. LPI Radar Waveforms

If the radar uses an FMCW waveform, the processing gain (apart from any noncoherent integration) is the sweep or modulation period t_m, multiplied by the sweep (input) bandwidth, ΔF (see Equation 1). That is:

$$PG_R = t_m \Delta F \tag{1}$$

The LPI receiver compresses (correlates) the received signal from the target using the stored reference signal, for the purpose of performing target detection. The correlation receiver is a 'matched receiver' if the reference signal is exactly the same duration as the finite duration return signal. Linear frequency-modulated (LFM) signals are the most significant example of waveform used in low probability of intercept (LPI) radars [SWI21].

A low probability of intercept (LPI) radar that uses frequency hopping techniques changes the transmitting frequency in time over a wide bandwidth in order to prevent an intercept receiver from intercepting the waveform. FSK has advantages like large bandwidth and high peak to side lobe ratio in both Doppler domain and autocorrelation domain [VAR21]. The frequency slots used are chosen from a frequency hopping sequence, and it is this unknown sequence that gives the radar the advantage over the intercept receiver in terms of processing gain. The frequency sequence appears random to the intercept receiver, and so the possibility of it following the changes in frequency is remote [PAC09]. This prevents a jammer from reactively jamming the transmitted frequency. Frequency hopping radar performance depends only slightly on the code used, given that certain properties are met. This allows for a larger variety of codes, making it more difficult to intercept.

The frequency hopping radar waveform will be used for this paper.

1.3. Detection of LPI Radars: Intercept Receiver Overview

In this section we switch from the topic of LPI radars, to the topic of those devices that detect and characterize LPI radar signals – which are the intercept receivers.

The three main types of intercept receivers are: electronic intelligence (ELINT) receivers, radar warning receivers (RWRs), and electronic support (ES) receivers.

ELINT is the result of observing the signals transmitted by radar systems in order to acquire information about their capabilities: it is the remote sensing of remote sensors. Through electronic intelligence, it is possible to obtain valuable information while at the same time remaining remote from the radar itself [KUM25]. Identification is performed by comparing the intercepted signal signature against the signatures contained within its threat library [CLA13]. So, the underlying basic function of electronic intelligence is to determine the capabilities of the radar, so that decisions can be made as to what threat it poses [GRA11]. Electronic intelligence receivers are the least time critical of the three intercept receivers. The output of the electronic intelligence receiver can be analyzed through off-line software-based analysis tools.

RWRs are critical for giving nearly immediate warning if specific threat signals are received (e.g., illumination of an aircraft's warning receiver by the target tracking radar of a threatening system) [DEM24]. The warning receiver typically has poor sensitivity and feeds into a near-real-time processor that uses a few parameter measurements to identify a threat. Usually, rough direction (e.g., quadrant or octant) is determined for the threat and the operator has a crude display showing functional radar type, direction, and relative range (strong signals displayed as being nearer than weaker ones). This type of receiver does not provide the kind of output that is analyzed using the methods described later in this paper.

ES receivers encompass all actions necessary to provide the information required for immediate decisions involving electronic warfare operations, threat avoidance, targeting, and homing [ASC16], [WIL06].

1.4. Intercept Receiver Signal Analysis Techniques

This section describes some of the classical time-frequency analysis techniques as well as the reassignment method and the Hough transform employed in this paper.

1.5. Time-Frequency Analysis

Time-frequency signal analysis concerns the analysis and processing of signals with time-varying frequency content. Such signals are best represented by a time-frequency distribution, which is intended to show how the energy of the signal is distributed over the two-dimensional time-frequency plane [ZML16]. Processing of the signal may then exploit the features produced by the concentration of signal energy in two dimensions (time and frequency), instead of only one-dimension (time or frequency). Since noise tends to spread out evenly over the time-frequency domain, while signals concentrate their energies within limited time intervals and frequency bands; the local SNR of a noisy signal can be improved simply by using time-frequency analysis [BOA15]. Also, the intercept receiver can increase its processing gain by implementing time-frequency signal analysis [GHA20]. Time-frequency distributions are useful for the visual interpretation of signal dynamics, through which an experienced operator can quickly detect a signal and also extract the signal parameters by analyzing the time-frequency distribution [BOA15].

1.6. The Spectrogram

The spectrogram is defined as the magnitude squared of the STFT. For non-stationary signals, the STFT is usually in the form of the spectrogram [FLA15], [STS17].

The STFT of a signal $x(u)$ is given in Equation 2 as:

$$F_x(t,f;h) = \int_{-\infty}^{+\infty} x(u)h(u-t)e^{-j2\pi f u}du \tag{2}$$

Where $h(t)$ is a short time analysis window localized around $t = 0$ and $f = 0$. Because multiplication by the relatively short window $h(u-t)$ effectively suppresses the signal outside a neighborhood around the analysis point $u = t$, the STFT is a 'local' spectrum of the signal $x(u)$ around t. Think of the window $h(t)$ as sliding along the signal $x(u)$ and for each shift $h(u-t)$ we compute the usual Fourier transform of the product function $x(u)h(u-t)$. The observation window allows localization of the spectrum in time but also smears the spectrum in frequency in accordance with the uncertainty principle, leading to a trade-off between time resolution and frequency resolution. In general, if the window is short, the time resolution is good, but the frequency resolution is poor, and if the window is long, the frequency resolution is good, but the time resolution is poor.

The STFT was the first tool devised for analyzing a signal in both time and frequency simultaneously. For analysis of human speech, the main method was, and still is, the STFT. In general, the STFT is still the most widely used method for studying non-stationary signals [SAR24].

The spectrogram (the squared modulus of the STFT) is given by Equation 3 as:

$$S_x(t,f) = \left| \int_{-\infty}^{+\infty} x(u)h(u-t)e^{-j2\pi f u} du \right|^2 \tag{3}$$

The spectrogram is a real-valued and non-negative distribution. Since the window h of the STFT is assumed of unit energy, the spectrogram satisfies the global energy distribution property. Thus we can interpret the spectrogram as a measure of the energy of the signal contained in the time-frequency domain centered on the point (t,f) and whose shape is independent of this localization.

Here are some properties of the spectrogram: 1) time and frequency covariance - the spectrogram preserves time and frequency shifts, thus the spectrogram is an element of the class of quadratic time-frequency distributions that are covariant by translation in time and in frequency (i.e. Cohen's class); 2) time-frequency resolution - the time-frequency resolution of the spectrogram is limited exactly as it is for the STFT; there is a trade-off between time resolution and frequency resolution. This poor resolution is the main drawback of this representation; 3) interference structure - as it is a quadratic (or bilinear) representation, the spectrogram of the sum of two signals is not the sum of the two spectrograms (quadratic superposition principle); there is a cross-spectrogram part and a real part. Thus, as for every quadratic distribution, the spectrogram presents interference terms; however, those interference terms are restricted to those regions of the time-frequency plane where the signals overlap. Thus if the signal components are sufficiently distant so that their spectrograms do not overlap significantly, then the interference term will nearly be identically zero [FLA15].

1.7. The Wigner-Ville Distribution

One of the members of the time-frequency analysis techniques family is the Wigner-Ville Distribution (WVD). The WVD has several desirable mathematical properties: it is always real-valued, it preserves time and frequency shifts, and it satisfies marginal properties [BOA15]. The WVD is computed by correlating the signal with a time and frequency translated version of itself, making it bilinear. The WVD has the highest signal energy concentration in the time-frequency plane [DEB14]. By using the WVD, an intercept receiver can come close to having a processing gain near the LPI radar's matched filter processing gain [PAC09]. The WVD, however, contains cross term interference between each pair of signal components, which may limit its applications, and which can make the WVD time-frequency representation hard to read, especially if the components are numerous or close to each other, and the more so in the presence of noise [KHA16]. This lack of readability may equate to less accurate signal detection and parameter extraction metrics, potentially placing the intercept receiver signal analyst's platform in harm's way.

The WVD of a signal $x(t)$ is given in Equation 4 as:

$$W_x(t,f) = \int_{-\infty}^{+\infty} x\left(t+\frac{\tau}{2}\right) x^*\left(t-\frac{\tau}{2}\right) e^{-j2\pi f \tau} d\tau \tag{4}$$

or equivalently in Equation 5 as:

$$W_x(t,f) = \int_{-\infty}^{+\infty} X\left(f+\frac{\xi}{2}\right) X^*\left(f-\frac{\xi}{2}\right) e^{j2\pi \xi t} d\xi \tag{5}$$

A lack of readability must be overcome to obtain time-frequency distributions that can be easily read by operators and easily included in a signal processing application [BOA15].

1.8. The Reassignment Method

Bilinear time-frequency distributions offer a wide range of methods designed for the analysis of non-stationary signals. Nevertheless, a significant point of these methods is their readability [ZHF22], which means both a good concentration of the signal components along with few misleading interference terms. A lack of readability, which is a known deficiency in the classical time-frequency analysis techniques, must be overcome in order to obtain time-frequency distributions that can be both easily read by non-experts and easily included in a signal processing application [BOA15]. Inability to obtain readable time-frequency distributions can lead to inaccurate signal metrics extraction, which in turn can bring about an uninformed and therefore potentially unsafe intercept receiver environment.

Some efforts have been made in that direction, and in particular, a general methodology referred to as reassignment.

The original idea of reassignment was introduced in an attempt to improve the Spectrogram [MIJ18]. As with any other bilinear energy distribution, the Spectrogram, as mentioned before, is faced with an unavoidable trade-off between the reduction of misleading interference terms and a sharp localization of the signal components.

We can define the Spectrogram as a two-dimensional convolution of the Wigner-Ville Distribution (WVD) of the signal by the WVD of the analysis window, as in Equation 6:

$$S_x(t,f;h) = \iint_{-\infty}^{+\infty} W_x(s,\xi) W_h(t-s, f-\xi) ds\, d\xi \tag{6}$$

Therefore, the distribution reduces the interference terms of the signal's WVD, but at the expense of time and frequency localization. However, a closer look at Equation 6 shows that $W_h(t-s, f-\xi)$ delimits a time-frequency domain at the vicinity of the (t,f) point, inside which a weighted average of the signal's WVD values is performed. The key point of the reassignment principle is that these values have no reason to be symmetrically distributed around (t,f), which is the geometrical center of this domain. Therefore, their average should not be assigned at this point, but rather at the center of gravity of this domain, which is much more representative of the local energy distribution of the signal. Reasoning with a mechanical analogy, the local energy distribution $W_h(t-s, f-\xi)W_x(s,\xi)$ (as a function of s and ξ) can be considered as a mass distribution, and it is much more accurate to assign the total mass (i.e. the Spectrogram value) to the center of gravity of the domain rather than to its geometrical center. Another way to look at it is this: the total mass of an object is assigned to its geometrical center, an arbitrary point which except in the very specific case of a homogeneous distribution, has no reason to suit the actual distribution. A much more meaningful choice is to assign the total mass of an object, as well as the Spectrogram value, to the center of gravity of their respective distribution [BOA15], [FAC18].

This is exactly how the reassignment method proceeds: it moves each value of the Spectrogram computed at any point (t,f) to another point $(\hat{t},\hat{f})$ which is the center of gravity of the signal energy distribution around (t,f) (see Equations 7 and 8) [MIB16]:

$$\hat{t}(x;t,f) = \frac{\iint_{-\infty}^{+\infty} s\, W_h(t-s, f-\xi)W_x(s,\xi) ds\, d\xi}{\iint_{-\infty}^{+\infty} W_h(t-s, f-\xi)W_x(s,\xi) ds\, d\xi} \tag{7}$$

$$\hat{f}(x;t,f) = \frac{\iint_{-\infty}^{+\infty} \xi\, W_h(t-s, f-\xi)W_x(s,\xi) ds\, d\xi}{\iint_{-\infty}^{+\infty} W_h(t-s, f-\xi)W_x(s,\xi) ds\, d\xi} \tag{8}$$

and thus leads to a reassigned Spectrogram (Equation 9), whose value at any point (t', f') is the sum of all the Spectrogram values reassigned to this point:

$$S_x^{(r)}(t', f'; h) = \iint_{-\infty}^{+\infty} S_x(t, f; h)\delta\left(t' - \hat{t}(x; t, f)\right)\delta\left(f' - \hat{f}(x; t, f)\right) dt\, df \tag{9}$$

One of the most interesting properties of this new distribution is that it also uses the phase information of the STFT, and not only its squared modulus as in the Spectrogram. It uses this information from the phase spectrum to sharpen the amplitude estimates in time and in frequency. This can be seen from the following expressions of the reassignment operators (Equations 10 and 11):

$$\hat{t}(x; t, f) = -\frac{d\Phi_x(t, f; h)}{df} \tag{10}$$

$$\hat{f}(x; t, f) = f + \frac{d\Phi_x(t, f; h)}{dt} \tag{11}$$

where $\Phi_x(t, f; h)$ is the phase of the STFT of $x : \Phi_x(t, f; h) = \arg(F_x(t, f; h))$. However, these expressions (Equations 10 and 11) do not lead to an efficient implementation, and have to be replaced by Equations 12 (local group delay) and 13 (local instantaneous frequency):

$$\hat{t}(x; t, f) = t - \Re\left\{\frac{F_x(t, f; T_h)F_x^*(t, f; h)}{|F_x(t, f; h)|^2}\right\} \tag{12}$$

$$\hat{f}(x; t, f) = f - \Im\left\{\frac{F_x(t, f; D_h)F_x^*(t, f; h)}{|F_x(t, f; h)|^2}\right\} \tag{13}$$

where $T_h(t) = t \times h(t)$ and $D_h(t) = \frac{dh}{dt}(t)$. This leads to an efficient implementation for the Reassigned Spectrogram without explicitly computing the partial derivatives of phase. The Reassigned Spectrogram may thus be computed by using 3 STFTs, each having a different window (the window function h; the same window with a weighted time ramp $t \times h$; and the derivative of the window function h with respect to time (dh/dt)). Reassigned Spectrograms are therefore very easy to implement, and do not require a drastic increase in computational complexity.

One of the most important properties of the reassignment method is that the application of the reassignment process to any distribution of Cohen's class theoretically yields perfectly localized distributions for chirp signals, frequency tones, and impulses, since the WVD does so also. This is one of the reasons that the reassignment method is a good choice as a signal process analysis tool for analyzing LPI radar waveforms such as triangular modulated FMCW waveforms (which can be viewed as back-to-back chirps) and FSK waveforms (which can be viewed as frequency tones).

The reassignment method provides readability improvement. The components are much better localized and more concentrated. In order to rectify the classical time-frequency analysis deficiency of poor time-frequency localization, there needs to be a method that produces more concentrated distributions, which the reassignment method does. This squeezing quality of the reassignment method lead to improved readability - which leads to more accurate metrics extracted – which in turn, creates a more informed and safer intercept receiver environment.

The reassignment principle for the Spectrogram allows for a straight-forward extension of its use to other distributions as well [BOA15], [FAC18]. If we consider the general expression of a distribution of the Cohen's class as a two-dimensional convolution of the WVD, as in Equation 14:

$$C_x(t, f; \Pi) = \iint_{-\infty}^{+\infty} \Pi(t - s, f - \xi)W_x(s, \xi) ds\, d\xi \tag{14}$$

replacing the particular smoothing kernel $W_h(u, \xi)$ by an arbitrary kernel $\Pi(s, \xi)$ simply defines the reassignment of any member of Cohen's class (Equations 15 through 17):

$$\hat{t}(x; t, f) = \frac{\iint_{-\infty}^{+\infty} s\, \Pi(t - s, f - \xi)W_x(s, \xi) ds\, d\xi}{\iint_{-\infty}^{+\infty} \Pi(t - s, f - \xi)W_x(s, \xi) ds\, d\xi} \tag{15}$$

$$\hat{f}(x; t, f) = \frac{\iint_{-\infty}^{+\infty} \xi\, \Pi(t - s, f - \xi)W_x(s, \xi) ds\, d\xi}{\iint_{-\infty}^{+\infty} \Pi(t - s, f - \xi)W_x(s, \xi) ds\, d\xi} \tag{16}$$

$$C_x^{(r)}(t', f'; \Pi) = \iint_{-\infty}^{+\infty} C_x(t, f; \Pi)\delta\left(t' - \hat{t}(x; t, f)\right)\delta\left(f' - \hat{f}(x; t, f)\right) dt\, df \tag{17}$$

The resulting reassigned distributions efficiently combine a reduction of the interference terms provided by a well-adapted smoothing kernel and an increased concentration of the signal components achieved by the reassignment. In addition, the reassignment operators $\hat{t}(x; t, f)$ and $\hat{f}(x; t, f)$ are almost as easy to compute as for the Spectrogram [YUG19].

Again, for Cohen's class, it can be shown that these modified distributions are also theoretically perfectly localized for chirps and impulses.

Once again, the smoothing and squeezing qualities of the reassignment method lead to improved readability, which in turn leads to more accurate metrics extraction, which may create a more informed and safer intercept receiver environment.

The reassignment method utilized in this paper is the Reassigned Smoothed Pseudo Wigner Ville Distribution (RSPWVD).

1.9. The Hough Transform

P.V.C. Hough patented the Hough Transform (HT) in 1962, and it was later used in work accomplished by Duda and Hart [MUK15].

Consider the case where we have straight lines in an image. For every point (x_i, y_i) in the image, all the straight lines pass through that point satisfy $y_i = mx_i + c$ for varying values of line slope and intercept.

Now if we reverse our variables and look instead at the values of (m, c) as a function of the image point coordinates (x_i, y_i), then $y_i = mx_i + c$ becomes $c = y_i - mx_i$ which also describes a straight line.

Consider two points p_1 and p_2, which lie on the same line in the (x, y) space. For each point, we can represent all possible lines through it by a single line in the (m, c) space. Therefore a line in the (x, y) space that passes through both points must lie on the intersection of the two lines in the (m, c) space representing the two points. This means that all points which lie on the same line in the (x, y) space are represented by lines which all pass through a single point in the (m, c) space.

To avoid the problem of infinite m values which occur when vertical lines exist in the image, an alternative formulation, $\rho = x\cos\theta + y\sin\theta$ (the parametric representation of a line) can be used to describe a line [DAH08]. This means that a point in the (x, y) space (image space) is now represented by a sinusoid in (ρ, θ) space (parameter space) rather than by a straight line. Points lying on the same line in the (x, y) space define sinusoids in the parameter space which all intersect at the same point. The more points that exist on that particular line in image space; the more sinusoids will intercept at that particular point in parameter space, and consequently, the more the accumulator value at this point (parameter space) will increase, forming a 'spike' in the parameter space. Therefore, 'spikes' (peak values) in the parameter space correspond to lines in the image space. The coordinates of the point of intersection of the sinusoids in the parameter space define the parameters of the line in the (x, y) space (image space). For example, if we apply the Hough transform to the RSPWVD of a chirp (line), we obtain a peak in the parameter space located in a position which depends on the parameter values (such as chirp rate) of the chirp (line) in the image space (the RSPWVD plot) [ERD17].

This can best be shown by Figure 1 below:

In Figure 1, the image space (time-frequency plot) is on the left and the parameter space (two-dimensional Hough transform plot) is on the right. Each point in the image space maps to a sinusoidal curve in the parameter space. The points 1, 2, and 3 in the image space map to the sinusoidal curves 1, 2, and 3 in the parameter space. In the parameter space, the intersection of the sinusoidal curves 1, 2, 3 at the point $\rho(x)$, $\theta(x)$ corresponds to the line connecting the points 1, 2, and 3 in the image space (same $\rho(x)$ and $\theta(x)$ values). The more sinusoidal curves in the parameter space that pass through a particular point, the higher the accumulator value of that point will be and the higher the three-dimensional Hough Transform 'spike' will be [SEI18]. The presence of a peak in the parameter space reveals the presence of high positive values concentrated along a line in the image space – whose parameters are exactly the coordinates of the peak. The peak in the parameter space is located in a position which depends on the chirp rate of the line in the image space [SON05]. The two-dimensional Hough transform plot is simply a birds-eye view of the three-dimensional plot, therefore a 'point' (or 'bright spot') in two-dimensional Hough transform plot is equivalent to a 'spike' in the three-dimensional Hough transform plot. The Hough transform converts a difficult global detection problem in the image space into a more easily solved local peak detection problem in the parameter space [SON05].

The Hough Transform of a given function $g(x, y)$ is defined in Equation 18 as:

$$H_g(\rho, \theta) = \iint_{-\infty}^{+\infty} g(x, y)\delta(\rho - x\cos\theta - y\sin\theta)\, dx\, dy \tag{18}$$

Where δ is the Dirac delta function. With $g(x, y)$ (as noted in the figure above), each point (x, y) in the original image g, is transformed into a sinusoid $\rho = x\cos\theta + y\sin\theta$, where, in the image, ρ is the perpendicular distance from the center of the image to the line at an angle θ from the vertical axis passing through the center of the image. Again, points that lie on the same line in the image will produce sinusoids that all cross at a single point in the Hough plot.

The expression above gives the projection (line integral) of $g(x, y)$ along an arbitrary line in the xy plane. By definition, the Hough transform computes the integration of the values of an image over all its lines.

From the signal location (rho and theta values) of the Hough transform plot, it is possible to back-map back to the signal location in the time-frequency representation, using the same exact rho and theta values.

Back-mapping example #1: HT of RSPWVD vs. RSPWVD - for a Triangular Modulated FMCW (TriModFMCW) waveform. (Note: a back-mapping example can be done for the HT of any of Cohen's class Time-Frequency Distributions, with any waveform composed of straight lines (i.e. TriModFMCW, FSK-4 component, FSK-8-component, etc.)).

Starting with the HT plot in Figure 2 (below):

The 4 signals are clearly seen in the Hough transform plot (Figure 2); from left to right the signal values are (theta, rho):

Signal 4: 0.7854, 136
Signal 3: 2.381, 43.22
Signal 2: 3.902, 43.93
Signal 1: 5.498, 136.7

These values of rho and theta allow for back-mapping to the time-frequency distribution in order to determine the location of these 4 signals in the time-frequency distribution.

Theta is in radians; therefore we multiply by 57.3 to obtain degrees.

Rho is the number of samples; therefore we divide by 360 (the number of samples of the Y-Axis of the HT plot) in order to obtain rho (length) in terms of percent of the length of the entire Y-Axis (of the time-frequency distribution).

Based on this:

Signal 4: 45.0 degrees, 38% of Y-Axis
Signal 3: 136.4 degrees, 12% of Y-Axis
Signal 2: 223.6 degrees, 12% of Y-Axis
Signal 1: 315.0 degrees, 38% of Y-Axis

With these values, we can now back-map from the Hough transform plot above (Figure 2) to the time-frequency distribution plot below (Figure 3) in order to find where the 4 signals are located.

Back-mapping example #2: HT of RSPWVD vs. RSPWVD - for an FSK-4 component waveform. (Again - Note: a back-mapping example can be done for the HT of any of Cohen's class Time-Frequency Distributions, with any waveform composed of straight lines (i.e. TriModFMCW, FSK-4 component, FSK-8-component, etc.)).

Starting with the HT plot in Figure 4 (below):

The 4 signals are clearly seen in the Hough transform plot (Figure 4); from left to right the signal values are (theta, rho):

Signal 2: 0.012, 104.0
Signal 3: 3.154, 102.7
Signal 1: 3.154, 51.01
Signal 4: 3.166, 3.1

These values of rho and theta allow for back-mapping to the time-frequency distribution in order to determine the location of these 4 signals in the time-frequency distribution.

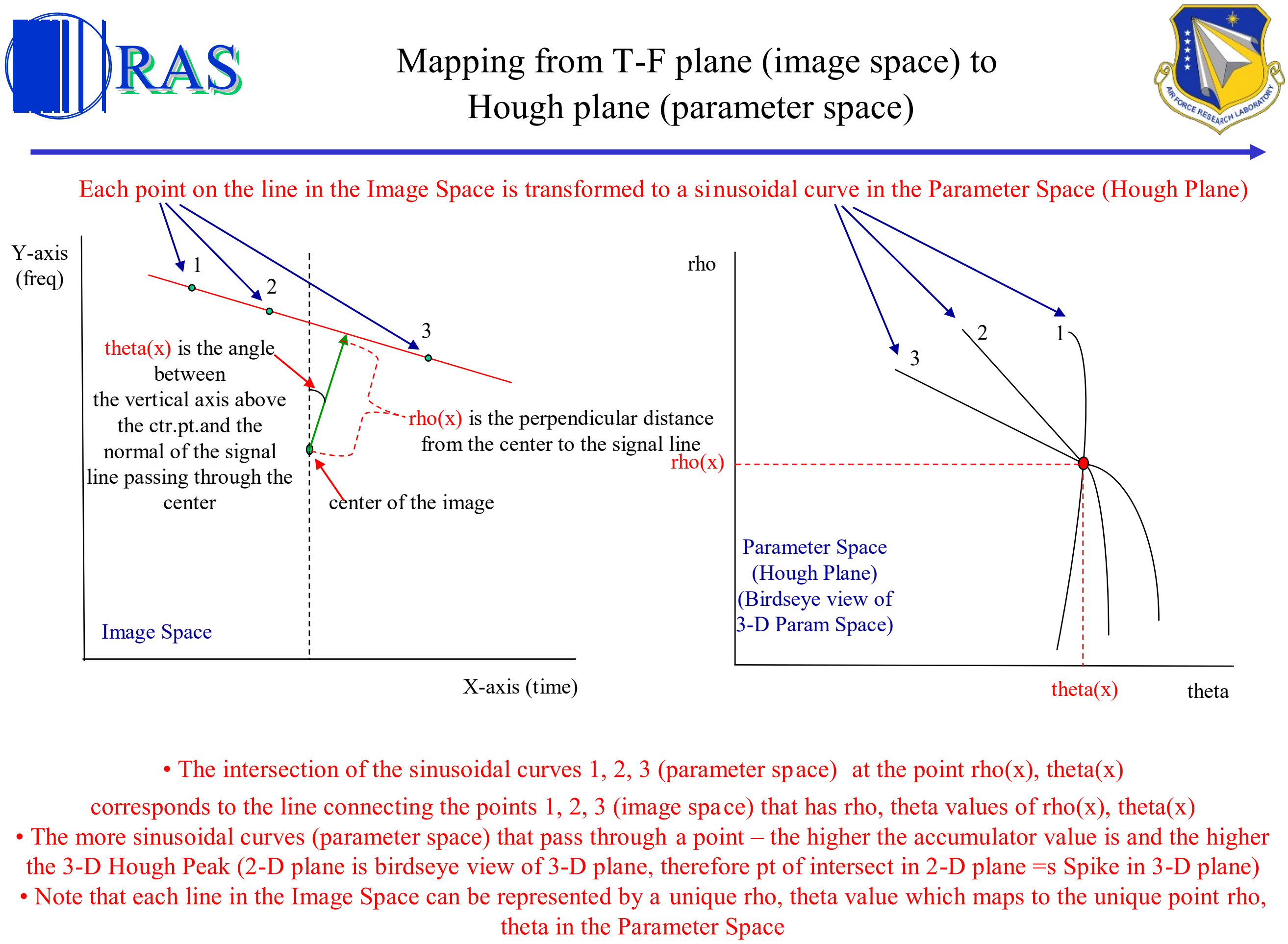

Figure 1. Time-frequency plot on the left and Hough transform plot on the right. A point in the TF plot maps to a sinusoidal curve in the HT plot. A line (signal) in the TF plot maps to a point in the HT plot. The rho and theta values of the point in the HT plot can be used to back-map to the TF plot in order to find the location of the line (signal) (good if time-frequency plot is cluttered with noise and/or cross-term interference and signal is not visible).

Theta is in radians, therefore we multiply by 57.3 to obtain degrees.

Rho is the number of samples, therefore we divide by 360 (the number of samples of the Y-Axis of the HT plot) in order to obtain rho (length) in terms of percent of the length of the entire Y-Axis (of the time-frequency distribution).

Based on this:

Signal 2: 0 degrees, 29% of Y-Axis
Signal 3: 180 degrees, 28% of Y-Axis
Signal 1: 180 degrees, 14% of Y-Axis
Signal 4: 180 degrees, 1% of Y-Axis

With these values, we can now back-map from the Hough transform plot above (Figure 4) to the time-frequency distribution plot below (Figure 5) in order to find where the 4 signals are located.

Figures 3 and 5 show how the unique theta and rho values from the Hough transform plot can be used to back-map to the time-frequency distribution in order to find the location of the signals in the time-frequency distribution. This would be beneficial in the case where the signals in the time-frequency distribution were unable to be seen, due to cross-term interference and/or noise, but the signals were able to be seen in the Hough transform plot.

It is important to note that the Hough transform method works well in the presence of multi-component signals, in spite of the cross-terms produced by time-frequency distributions such as the WVD [TOR07]. Since the cross-terms have an amplitude modulation, the integration implicit in the Hough transform reduces them, while the useful contributions, which are always positive, are correctly integrated [KIS15]. Likewise, in the presence of noise, the integration carried out by the Hough transform produces an improvement in the SNR [AVE18].

The Hough transform is similar to the Radon transform. The Hough transform, like the Radon transform is a mapping from image space to parameter space. The Radon transform is usually treated as a reading paradigm (how a data point in the destination space is obtained from the data in the source space). The Hough transform is usually treated as a writing paradigm (how a data point in the source space maps onto data points in the destination space) [GIN04].

Some additional advantages of the Hough transform are its ability to discard features belonging to other objects and its robustness against incomplete data [HAS15].

The Hough transform finds many uses today, from signal processing (such as low SNR signal extraction and chirp rate

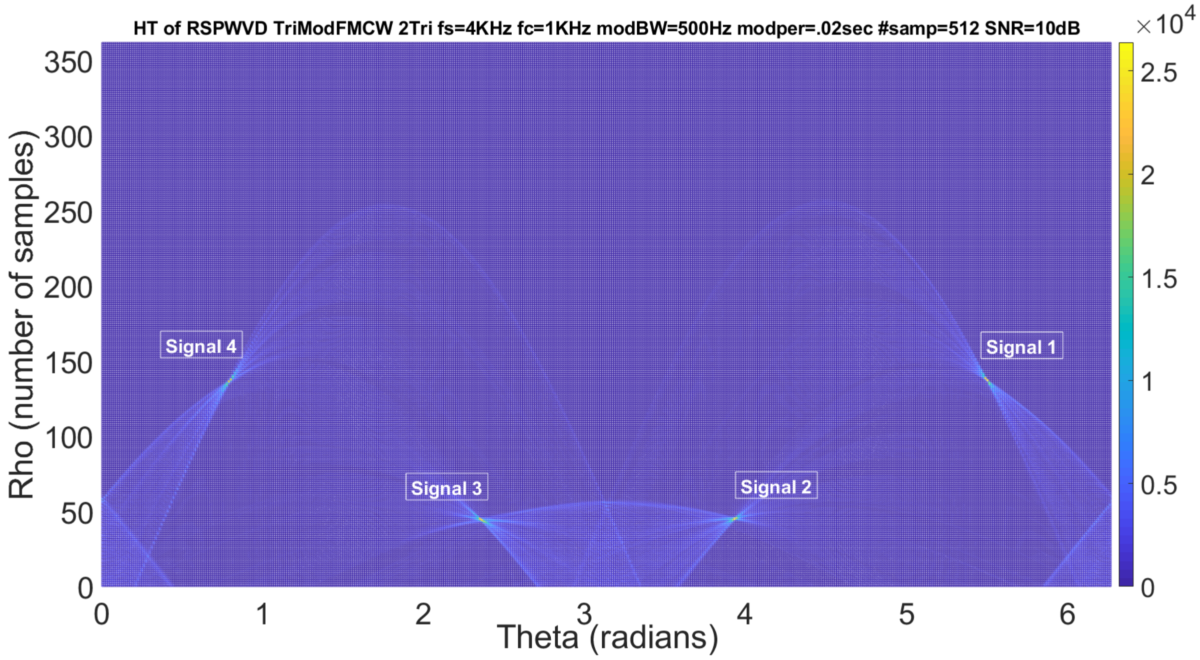

Figure 2. Hough transform of the RSPWVD of a triangular modulated FMCW signal at an SNR of 10dB (512 samples). Each point has a unique theta and rho value which can be used to back-map to the time-frequency (RSPWVD) representation in order to locate the 4 signals, as depicted in Figure 3.

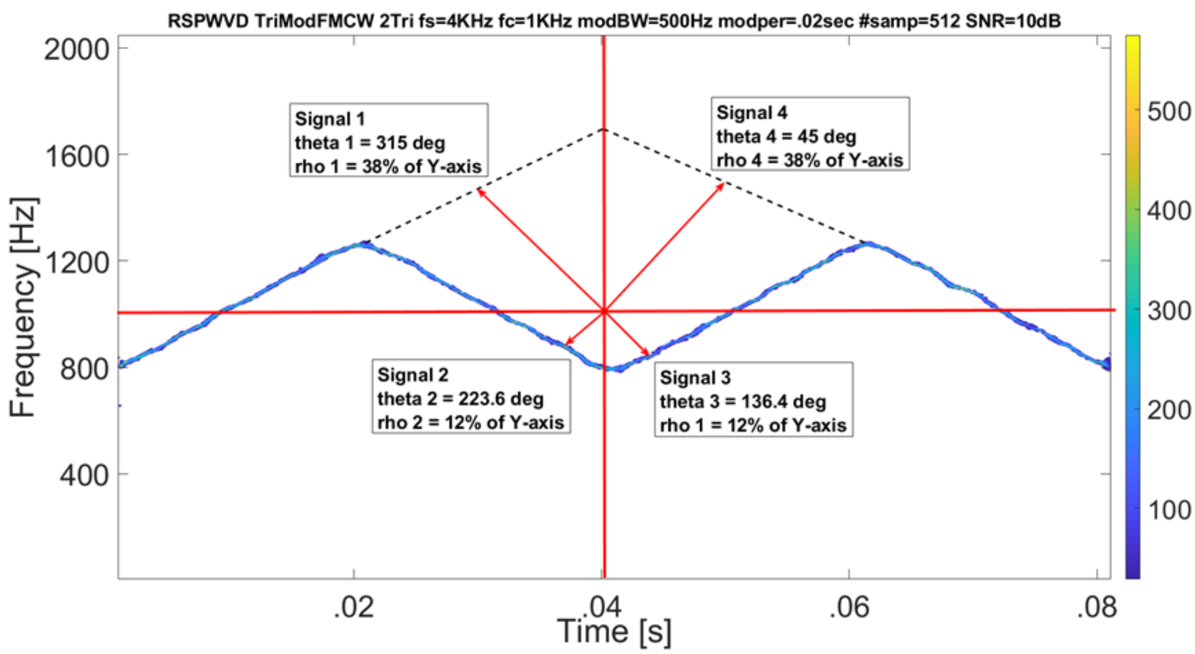

Figure 3. The unique theta and rho values extracted from Figure 2 are used to back-map to the time-frequency representation (RSPWVD of a triangular modulated FMCW signal (SNR=10dB, #samples=512)) in order to locate the 4 chirp signals that make up the 4 legs of the triangular modulated FMCW signal.

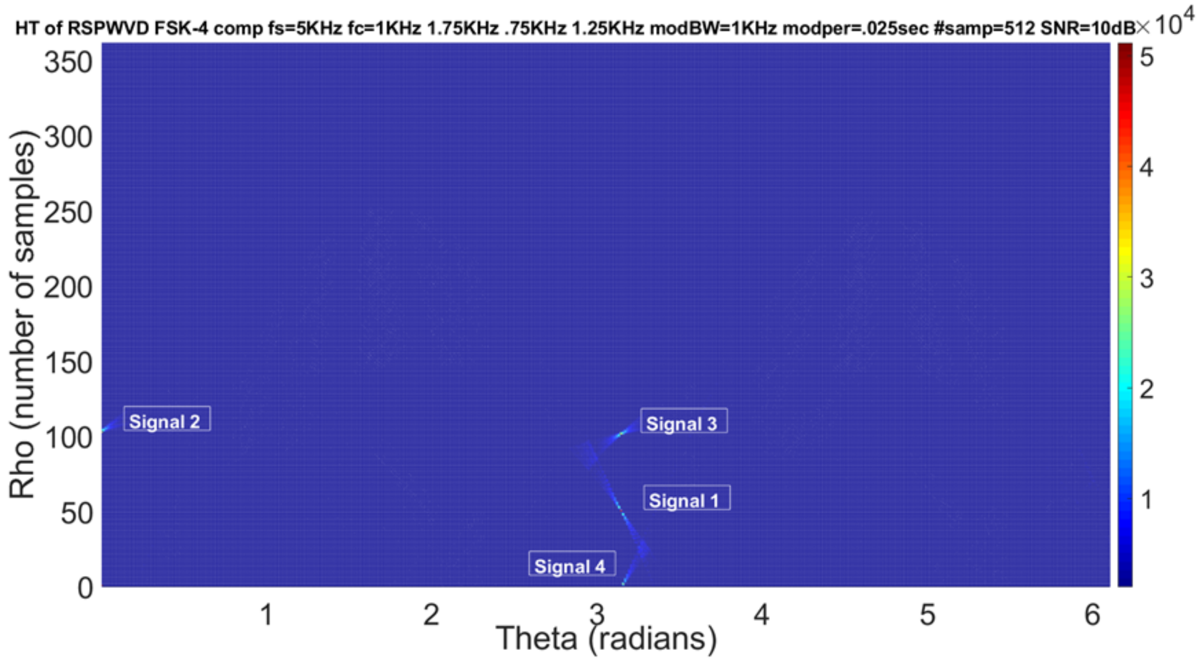

Figure 4. Hough transform of the RSPWVD of an FSK-4 component signal at an SNR of 10dB (512 samples). Each point has a unique theta and rho value which can be used to back-map to the time-frequency (RSPWVD) representation in order to locate the 4 signals, as depicted in Figure 5.

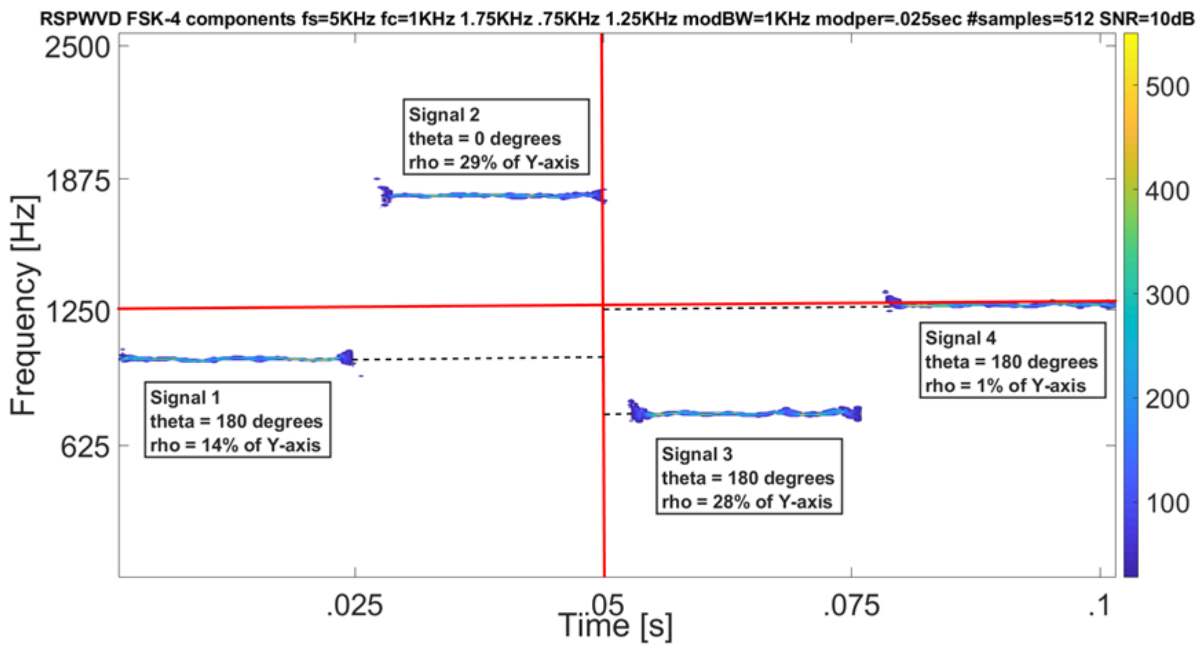

Figure 5. The unique theta and rho values extracted from Figure 4 are used to back-map to the time-frequency representation (RSPWVD of an FSK-4 component signal (SNR=10dB, #samples=512)) in order to locate the 4 chirp signals that make up the 4 legs of the FSK-4 component signal.

determination) to image processing (such as locating iris features in frontal face images [SIN15]).

The ability of the Hough Transform to perform well in low SNR environments as well as in heavy cross-term environments makes it an ideal signal analysis tool to offset the classical time-frequency analysis deficiencies of cross-term interference and mediocre performance in low SNR environments. This will make for better readability, leading to more accurate parameter extractions for the intercept receiver signal analyst.

The Hough transform of the reassigned smoothed pseudo Wigner-Ville distribution (RSPWVD) is used in this paper.

2. Methodology

The methodologies detailed in this section describe the processes involved in obtaining and comparing metrics between the time-frequency analysis techniques of the Reassigned Smoothed Pseudo Wigner-Ville Distribution and the Hough Transform vs. the Reassigned Smoothed Pseudo Wigner-Ville Distribution for the detection of low probability of intercept frequency shift keying Radar signals in high noise environments.

The tools used for this testing were: Matrix Laboratory (MATLAB) (version 8.3), Signal Processing Toolbox (version 6.21), Wavelet Toolbox (version 4.7), Image Processing Toolbox (version 7.2), and Time-Frequency Toolbox (version 1.0) (http://tftb.nongnu.org/).

All testing was accomplished on a laptop computer (HP EliteBook; Processor - AMD Ryzen 7 PRO 7730U with Radeon Graphics 2.00 GHz. Installed RAM - 64.0 GB; System Type - 64-bit operating system, x64-based processor).

Testing was performed for the 4-component frequency hopping waveform (prevalent in the LPI arena [MAZ20]), with parameters of: sampling frequency=5KHz; carrier frequencies=1KHz, 1.75KHz, 0.75KHz, 1.25KHz; modulation bandwidth=1KHz; modulation period=.025sec. Waveform parameters were chosen for academic validation of signal processing techniques. Due to computer processing resources they were not meant to represent real-world values. The number of samples for each test was chosen to be 512, which seemed to be the optimum size for the laptop computer. Testing was performed at three different SNR levels: 10dB, 0dB, and the lowest SNR at which the signal could be detected. The noise added was white Gaussian noise, which best reflects the thermal noise present in the IF section of an intercept receiver [PAC09]. Kaiser windowing was used, when windowing was applicable. 100 runs were performed for each test, for statistical purposes. Unless otherwise indicated, the plots included in this paper were done at a threshold of 5% of the maximum intensity and were linear scale (not dB) of analytic (complex) signals; the color bar represents intensity. The signal processing tools used for each task were the Reassigned Smoothed Pseudo Wigner-Ville Distribution and the Hough Transform vs. the Reassigned Smoothed Pseudo Wigner-Ville Distribution.

After each particular run of each test, metrics were extracted from the time-frequency representation. The different metrics extracted were as follows:

1. **Percent detection:** Percent of time the signal was detected. A signal was declared a detection if any portion of each of the 4 FSK signal components exceeded a set detection threshold (a certain percentage of the maximum intensity) of the time-frequency representation - and - of the Hough transform representation.

   Detection threshold percentages were determined based on visual detections of low SNR signals (lowest SNR at which the signal could be visually detected in the time-frequency representation - and - in the Hough transform representation). For each of these low SNR plots - the peak intensity value for each of the 4 signal legs was recorded - and the lowest of these 4 values was documented. This process was repeated for 50 different plots, and the average of the lowest values was calculated, and assigned as the detection threshold percentage. For the RSPWVD, the detection threshold percentage was determined to be 50% - and - for the HT of RSPWVD, the detection threshold percentage was determined to be 20%.

   For percent detection determination, these detection threshold percentage values were included in the time-frequency plot algorithms and in the Hough transform plot algorithms, so that the detection thresholds could be applied automatically during the plotting process. From the percent detection plot, the signal was declared a detection if any portion of each of the 4 signal components was visible (see Figure 6 and Figure 7 below).

2. **Lowest detectable SNR:** The lowest SNR level at which at least a portion of each of the 4 FSK signal components exceeded a set detection threshold (a certain percentage of the maximum intensity) of the time-frequency representation - and - of the Hough transform representation, as determined above. The RSPWVD detection threshold percentage was determined to be 50% - and - the HT of RSPWVD detection threshold percentage was determined to be 20%.

   For the lowest detectable SNR determination, these detection threshold values were included in the time-frequency plot algorithms - and - in the Hough transform plot algorithms, so that the detection thresholds could be applied automatically during the plotting process. From the lowest detectable SNR plot, the signal was declared a detection if any portion of each of the 4 signal components was visible (see Figure 8 and Figure 9 below). The lowest SNR level for which the signal was declared a detection is the lowest detectable SNR value.

The data from all 100 runs for each test was used to produce the metrics listed below in the Results section. The metrics from the RSPWVD + HT were then compared to the metrics from the RSPWVD. By and large, the RSPWVD + HT outperformed the RSPWVD, as will be shown in the Results section.

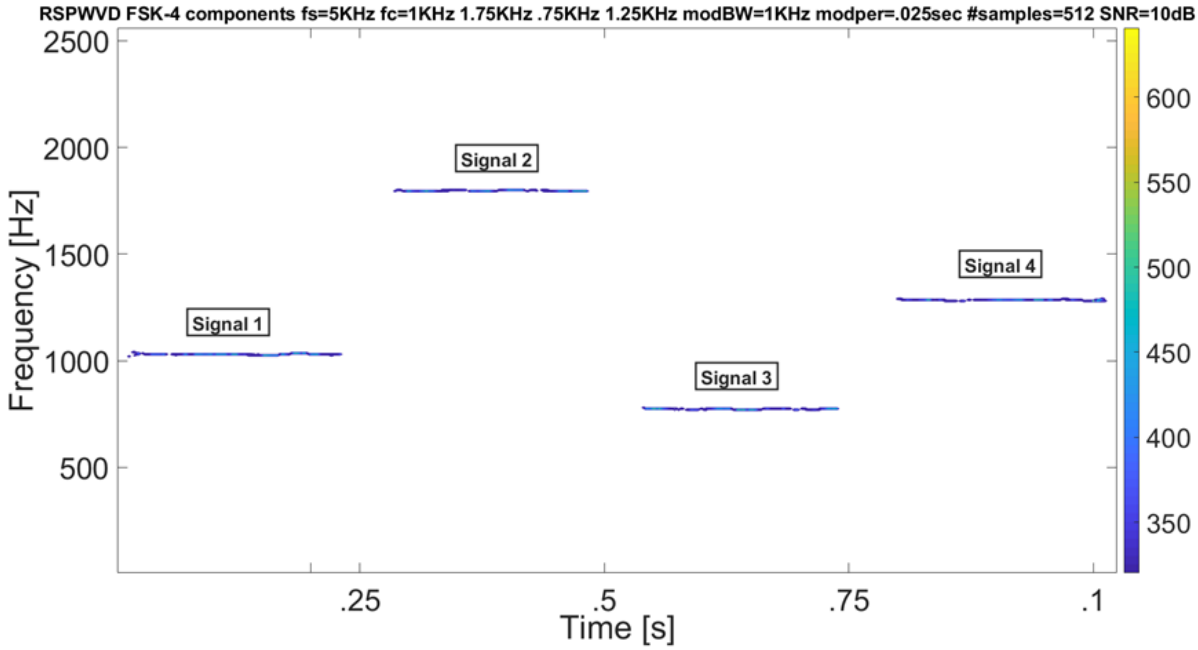

Figure 6. Example plot for determination of percent detection. This plot is a frequency vs. time plot of an RSPWVD of an FSK-4 component signal (SNR=10dB) with the detection threshold automatically set at 50%. From this plot, the signal was declared a (visual) detection because at least a portion of each of the 4 signal components was visible.

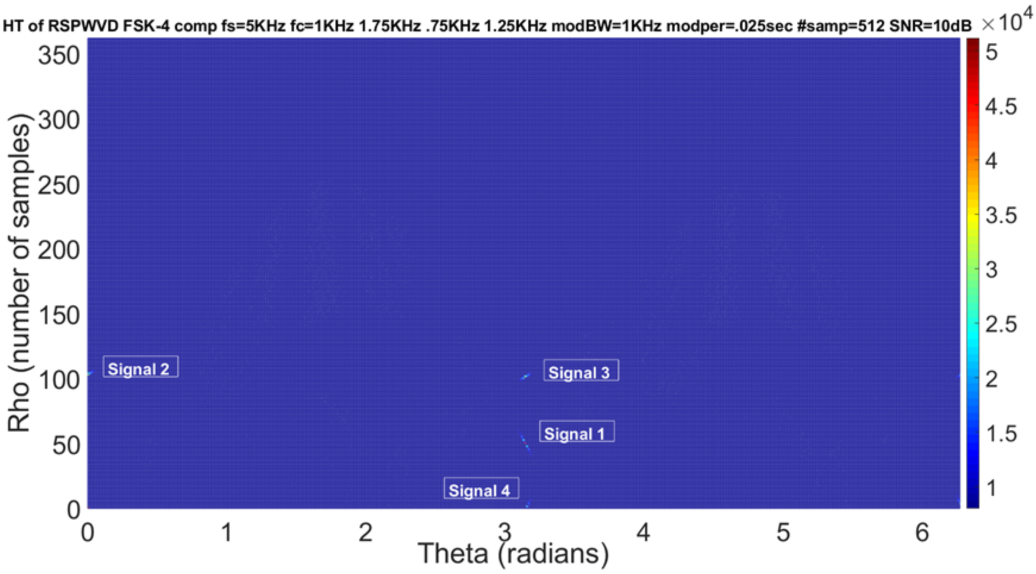

Figure 7. Example plot for determination of percent detection. This plot is a frequency vs. time plot of an HT of RSPWVD of an FSK-4 component signal (SNR=10dB) with the detection threshold automatically set at 20%. From this plot, the signal was declared a (visual) detection because at least a portion of each of the 4 signal components was visible.

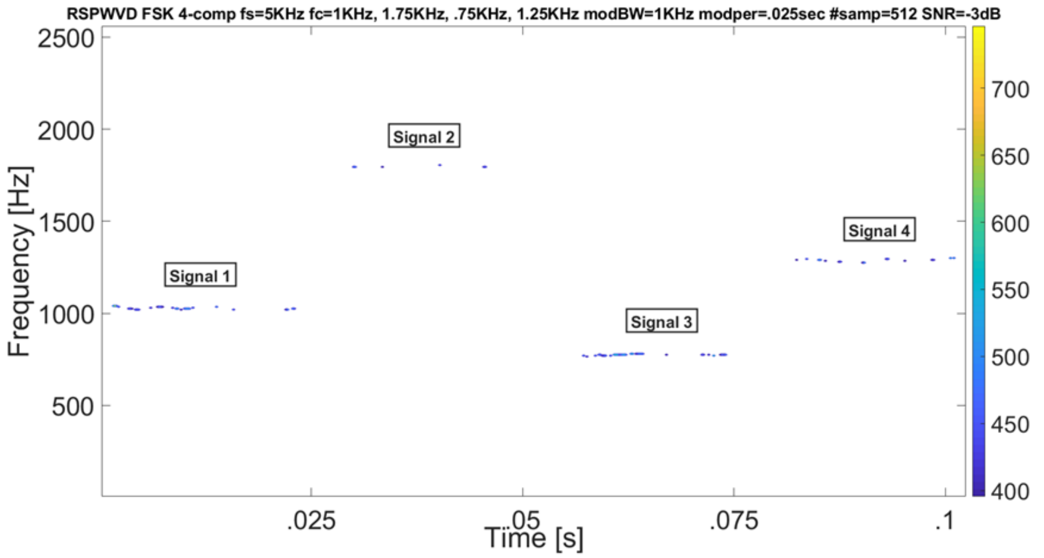

Figure 8. Lowest detectable SNR. This plot is a time vs. frequency (x-y view) of the RSPWVD of a 4-component frequency hopping signal (512 samples, SNR= -3dB) with the detection threshold automatically set at 50%. From this plot, the signal was declared a (visual) detection because at least a portion of each of the 4 frequency hopping signal components was visible. Compare to Figure 6, which is the same plot, except that it has an SNR level equal to 10dB.

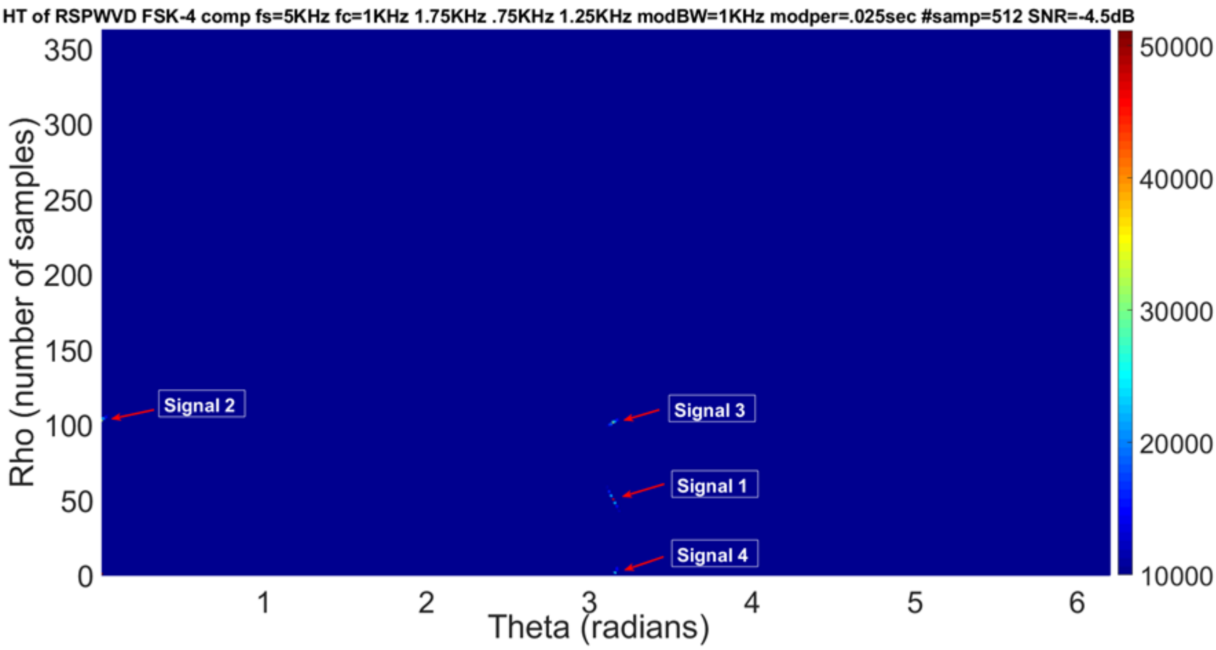

Figure 9. Lowest detectable SNR. This plot is a time vs. frequency (x-y view) of the HT of RSPWVD of a 4-component frequency hopping signal (512 samples, SNR= -4.5dB) with the detection threshold automatically set at 20%. From this plot, the signal was declared a (visual) detection because at least a portion of each of the 4 frequency hopping signal components was visible. Compare to Figure 7, which is the same plot, but with an SNR level equal to 10dB.

3. Results

Table 1 shows the overall test metrics for the Reassigned Smoothed Pseudo Wigner Ville Distribution (RSPWVD) vs. the Reassigned Smoothed Pseudo Wigner-Ville Distribution + Hough transform (RSPWVD + HT), for lowest detectable SNR (Low SNR) and percent detection (% Detection).

Table 1. Overall test metrics for the Reassigned Smoothed Pseudo Wigner Ville Distribution (RSPWVD) vs. the Reassigned Smoothed Pseudo Wigner-Ville Distribution + Hough transform (RSPWVD + HT). The parameters extracted are listed in the left-hand column: lowest detectable SNR (Low SNR), and percent detection (% Detection).

Parameters Extracted	RSPWVD	RSPWVD + HT
Low SNR	-3.0dB	-4.5dB
% Detection	92.9%	98.8%

From the test metrics in Table 1, it is seen that the RSPWVD + HT outperformed the HT in both Low SNR (-4.5dB vs. -3.0dB) and Percent Detection (98.8% vs. 92.9%).

Figure 10 shows comparative plots of the RSPWVD vs. the RSPWVD + HT (4-component FSK signal) at SNRs of 10dB (top 2 rows), 0dB (middle 2 rows), and lowest detectable SNR (bottom 2 rows).

4. Discussion

This section will elaborate on the results from the previous section.

From Table 1, it is seen that the RSPWVD + HT outperformed the HT in both Low SNR (-4.5dB vs. -3.0dB) and Percent Detection (98.8% vs. 92.9%).

These metrics are representative of: the good Low SNR and Percent Detection metrics for the Reassignment Method, due to its smoothing and squeezing qualities – and – the even better Low SNR and Percent Detection metrics for the RSPWVD + HT – with the addition of the Hough Transform's good performance in low SNR environments – both of which were discussed in earlier sections of this paper.

Consequently, the joint use of the Reassignment Method and the Hough Transform allows for more accurate signal detection of LPI radar signals (particularly in low SNR environs) than the RM alone, making for an even more informed, effective, and safer intercept receiver environment, which could potentially save valuable equipment, intelligence, and lives.

The RSPWVD might be used in a scenario where you need good signal localization in a fairly low SNR environment, whereas the RSPWVD + HT might be used in a scenario where you need very good signal detection/localization in a very low SNR environment.

5. Conclusions

Digital intercept receivers, whose main job is to detect and extract parameters from low probability of intercept radar signals, are currently moving away from Fourier-based analysis and moving towards classical time-frequency analysis techniques, such as the WVD and the RSPWVD, and also the Hough Transform, for the purpose of analyzing low probability of intercept radar signals. Based on the research performed for this paper (the novel direct comparison of the RSPWVD versus the RSPWVD + HT for the signal analysis of low probability of intercept frequency hopping radar signals) it was shown that the RSPWVD + HT by and large outperformed the RSPWVD for analyzing these low probability of intercept radar signals – for reasons brought out in the discussion section above. More accurate metrics may well equate to saved equipment and lives.

Future plans include analysis of an additional low probability of intercept radar waveform 8-component FSK signal, again using the RSPWVD and the RSPWVD + HT as time-frequency analysis techniques.

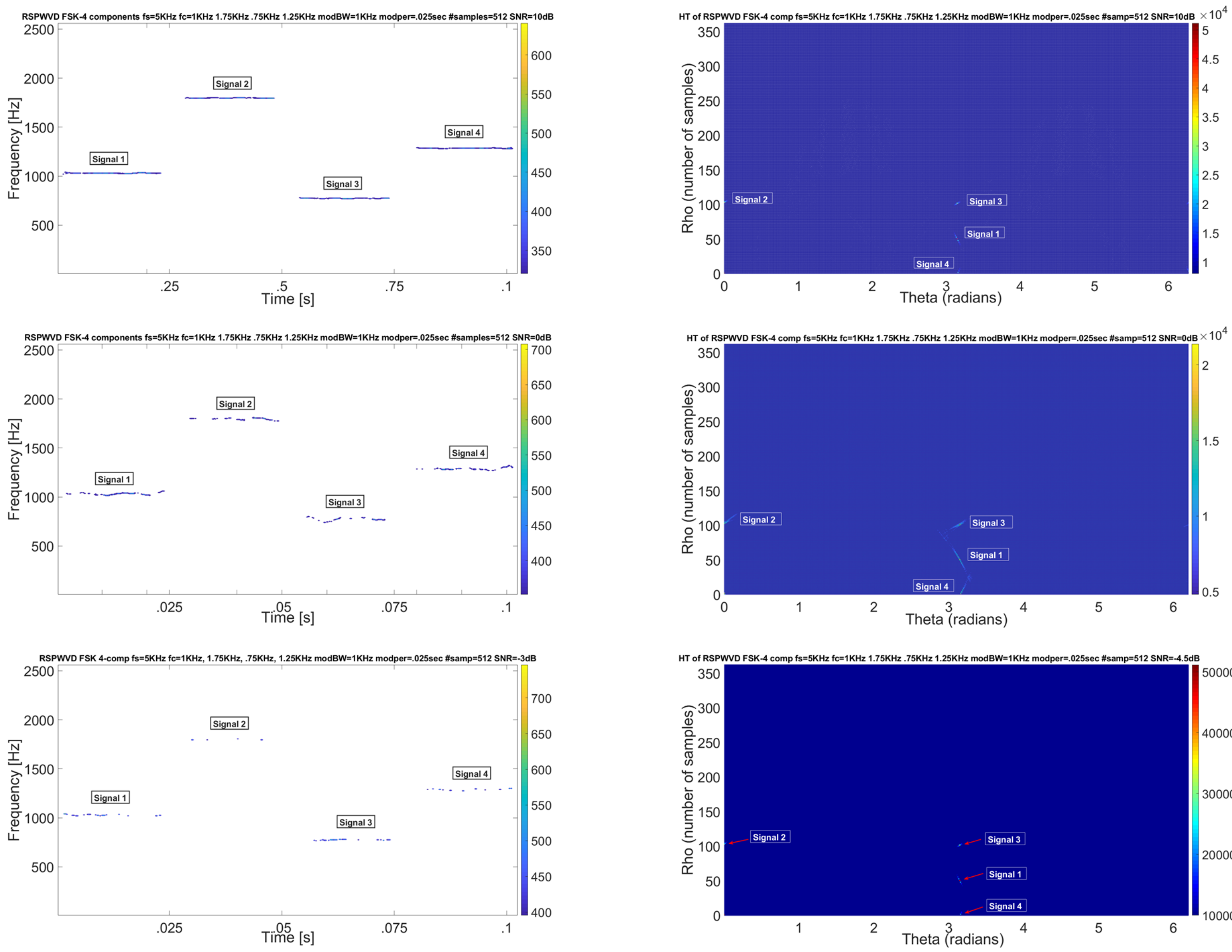

Figure 10. Comparative plots for a 4-component FSK low probability of intercept radar signals. The top 2 rows are at an SNR of 10dB (RSPWVD (with the detection threshold automatically set at 50%), then under it, HT of RSPWVD (with the detection threshold automatically set at 20%)). The middle 2 rows are at an SNR of 0dB (RSPWVD (with the detection threshold automatically set at 50%), then under it, HT of RSPWVD (with the detection threshold automatically set at 20%)). The bottom 2 rows are at the lowest SNR levels (RSPWVD (-3dB) (with the detection threshold automatically set at 50%), then under it, HT of RSPWVD (-4.5dB) (with the detection threshold automatically set at 20%)). The HT of RSPWVD outperformed the RSPWVD in percent detection and lowest detectable SNR, due to the HT's ability to dig signals out of noise.

REFERENCES

1. [ASC16] Apfeld, Sabine, Alexander Charlish, and Wolfgang Koch. "An adaptive receiver search strategy for electronic support." 2016 Sensor Signal Processing for Defence (SSPD). IEEE, 2016.

2. [AVE18] Averbuch G, Assink JD, Smets PS, Evers LG. "Extracting low signal-to-noise ratio events with the Hough transform from sparse array data." Geophysics. 2018 May 1;83(3): WC43-51.

3. [BOA15] Boashash, Boualem. "Time-frequency signal analysis and processing: a comprehensive reference." Academic press, 2015.

4. [CLA13] Clark, Robert M. "Intelligence collection." CQ Press, 2013.

5. [DAH08] Dahyot, R., Bayesian Classification for the Statistical Hough Transform. International Conference on Pattern Recognition, pp. 1-4, December 2008.

6. [DEB14] Debnath L, Shah FA. "The Wigner–Ville distribution and time–frequency signal analysis." In Wavelet Transforms and Their Applications 2014 Oct 25 (pp. 287-336). Boston, MA: Birkhäuser Boston.

7. [DEM24] Demircan M, Pakfiliz AG. "A novel machine learning approach for optimizing radar warning receiver preprogramming." Acadlore Trans. Mach. Learn. 2024 Oct;3(4):202-13.

8. [ERD17] Erdogan AY, Gulum TO, Durak-Ata L, Yildirim T, Pace PE. "FMCW signal detection and parameter extraction by cross Wigner–Hough transform." IEEE Transactions on Aerospace and Electronic Systems. 2017 Jan 9;53(1):334-44.

9. [FAC18] Flandrin, Patrick, Francois Auger, and Eric Chassande-Mottin. "Time-frequency reassignment: from principles to algorithms." Applications in time-frequency signal processing. CRC Press, 2018. 179-204.

10. [FLA15] Flandrin, Patrick. "Time–frequency filtering based on spectrogram zeros." IEEE Signal Processing Letters 22.11 (2015): 2137-2141.

11. [GHA20] Ghadimi, G., et al. ”Deep learning-based approach for low probability of intercept radar signal detection and classification.” Journal of Communications Technology and Electronics 65 (2020): 1179-1191.

12. [GIN04] Van Ginkel, M., Luengo Hendriks, C., Van Vliet, L., A Short Introduction to the Radon and Hough Transforms and How They Relate to Each Other. Technical Report QI-2004-01, Imaging Science and Technology Department, Delft University of Technology, The Netherlands, 2004.

13. [GRA11] Graham, Adrian. “Communications, radar and electronic warfare.” John Wiley & Sons, 2011.

14. [HAS15] Hassanein AS, Mohammad S, Sameer M, Ragab ME. “A survey on Hough transform, theory, techniques and applications.” arXiv preprint arXiv:1502.02160. 2015 Feb 7.

15. [KHA16] Khan NA, Sandsten M. “Time–frequency image enhancement based on interference suppression in Wigner–Ville distribution.” Signal Processing. 2016 Oct 1;127:80-5.

16. [KIS15] Kishore TR, Sidharth DS, Rao KD. “Analysis of linear and non-linear frequency modulated signals using STFT and hough transform.” In 2015 IEEE International Symposium on Signal Processing and Information Technology (ISSPIT) 2015 Dec 7 (pp. 490-494). IEEE.

17. [KUM25] Kumar RP. “Performance-Trade-Offs in ELINT Systems.” In 2025 4th International Conference on Range Technology (ICORT) 2025 Mar 6 (pp. 1-5). IEEE.

18. [LIX23] Liu, Xinyu, et al. ”Lpi radar waveform design with desired cyclic spectrum and pulse compression properties.” IEEE Transactions on Vehicular Technology (2023).

19. [MAZ20] Maziarz, J., et al. ”Frequency hopping signals in low probability of intercept radars.” Journal of Defense Electronics, 2020.

20. [MIB16] Mill, Robert W., and Guy J. Brown. ”Utilising temporal signal features in adverse noise conditions: Detection, estimation, and the reassigned spectrogram.” The Journal of the Acoustical Society of America 139.2 (2016): 904-917.

21. [MIJ18] Mika, Dariusz, and Jerzy Józwik. ”Advanced time-frequency representation in voice signal analysis.” Advances in Science and Technology. Research Journal 12.1 (2018).

22. [MUK15] Mukhopadhyay P, Chaudhuri BB. “A survey of Hough Transform. Pattern recognition.” 2015 Mar 1;48(3):993-1010.

23. [PAC09] Pace, Phillip E. “Detecting and classifying low probability of intercept radar.” Artech house, 2009.

24. [SAR24] Sarna ML, Hossain MR, Islam MA. “Comparative analysis of stft and wavelet transform in time-frequency analysis of non-stationary signals.” International Journal of Novel Research in Engineering and Science. 2024;11(1):72-8.

25. [SHC19] Shi, Chenguang, et al. ”Low probability of intercept-based optimal power allocation scheme for an integrated multistatic radar and communication system.” IEEE Systems Journal 14.1 (2019): 983-994.

26. [SEI18] Seifozzakerini S, Yau WY, Mao K, Nejati H. Hough transform implementation for event-based systems: Concepts and challenges. Frontiers in computational neuroscience. 2018 Dec 21; 12:103.

27. [SIN15] Singh S, Singh S. “Iris segmentation along with noise detection using Hough transform.” International Journal of Engineering and Technical Research (IJETR). 2015 May;3(5):440-4.

28. [SON05] Song J, Lyu MR. “A Hough transform based line recognition method utilizing both parameter space and image space.” Pattern recognition. 2005 Apr 1;38(4):539-52.

29. [SON22] Song, Yuxiao, et al. ”Ultra-low sidelobe waveforms design for LPI radar based on joint complementary phase-coding and optimized discrete frequency-coding.” Remote Sensing 14.11 (2022): 2592.

30. [STS17] Stevens, Daniel L., and Stephanie A. Schuckers. ”Low Probability of Intercept Triangular Modulated Frequency Modulated Continuous Wave Signal Characterization Comparison using the Spectrogram and the Scalogram.” Global Journals of Research in Engineering 17.F2 (2017): 37-47.

31. [SWI21] Swiercz E, Janczak D, Konopko K., “Detection of LFM radar signals and chirp rate estimation based on time-frequency rate distribution.” Sensors. 2021 Aug 10;21(16):5415.

32. [TOR07] Toronto, N., Morse, B., Ventura, D., Seppi, K., The Hough Transform’s Implicit Bayesian Foundation. IEEE International Conference on Image Processing, Vol. 4, pp. IV-377 – IV-380, October 2007.

33. [VAR21] Varma TA, Gera A. “Frequency Hopping Patterns for Low Probability of Intercept (LPI) Radars Using Costas Arrays.” In Optical and Wireless Technologies: Proceedings of OWT 2020 2021 Sep 2 (pp. 401-411). Singapore: Springer Singapore.

34. [WIL06] Wiley, Richard. ELINT: “The interception and analysis of radar signals.” Artech, 2006.

35. [WSQ19] Wang, Shi Qiang, et al. ”The background and significance of radar signal sorting research in modern warfare.” Procedia Computer Science 154 (2019): 519-523.

36. [YUA24] Yuan Y, Liu X, Zhang T, Cui G, Kong L. “Reinforcement-learning-enhanced adaption of signal power and modulation for LPI radar system.” IEEE Transactions on Aerospace and Electronic Systems. 2024 Jul 30;60(6):8555-68.

37. [YUG19] Yu, Gang, et al. ”Local maximum synchrosqueezing transform: An energy-concentrated time-frequency analysis tool.” Mechanical Systems and Signal Processing 117 (2019): 537-552.

38. [ZHF22] Zhang, Dong, and Zhipeng Feng. ”Enhancement of time-frequency post-processing readability for nonstationary signal analysis of rotating machinery: Principle and validation.” Mechanical Systems and Signal Processing 163 (2022): 108145.

39. [ZML16] Zhang, Ming, Lutao Liu, and Ming Diao. ”LPI radar waveform recognition based on time-frequency distribution.” Sensors 16.10 (2016): 1682.